RSC Advances

PAPER

View Article Online
View Journal | View Issue

Cite this: *RSC Adv.*, 2025, **15**, 23477

Sustainable and eco-friendly removal of 2,4,6-tricholorophenol from water using an acid-activated bio-waste/graphene oxide composite

Lina Adeida,[ab] Belkacem Benguella,[b] Makhoukhi Benamar[b] and Ayman H. Kamel *[ac]

The presence of 2,4,6-trichlorophenol (TCP) in aquatic systems presents considerable environmental and health risk owing to its persistence, toxicity, and bio-accumulative characteristics. In this work, an acid-activated eggshell/graphene oxide (AAES/GO) composite as an innovative and sustainable adsorbent was synthesized and characterized for the effective removal of TCP from aqueous solutions. The composite was synthesized *via* phosphoric acid activation of eggshells for surface modification, then incorporating graphene oxide for surface reactivity and adsorption capability enhancement. The thorough physicochemical analysis utilizing FTIR, SEM, EDX, and XRD validated the effective alteration and enhanced textural qualities of the AAES/GO composite. Adsorption experiments revealed fast adsorption of TCP, with a 63% removal accomplished in 10 min. The adsorption kinetics adhered to the pseudo-second-order model ($R^2 = 0.99$), signifying a chemically regulated adsorption process. Isotherm analysis indicated that the Temkin model ($R^2 = 0.92$) most accurately characterized the adsorption behavior, emphasizing the significance of surface interactions. The composite demonstrated elevated effectiveness with optimal adsorption at pH 6.5. Regeneration investigations demonstrated that the material could be re-utilized for a maximum of three cycles before experiencing a substantial decline in efficiency. The results indicate that the AAES/GO composite is a cost-effective, environmentally sustainable, and efficient adsorbent, presenting a viable alternative for the removal of TCP from contaminated water systems.

Received 8th April 2025
Accepted 1st July 2025

DOI: 10.1039/d5ra02424b

rsc.li/rsc-advances

Introduction

Chlorophenols are a group of organic compounds characterized by the presence of one or more chlorine atoms attached to a phenolic ring.[1] They are widely used in various industrial, agricultural, and household applications.[2] However, due to their persistence and toxicity, they are now recognized as significant environmental pollutants. Among them, 2,4,6-trichlorophenol (TCP) is of particular concern because of its chemical stability, inherent toxicity, and resistance to degradation.[3] TCP is typically released as an unintentional byproduct of combustion processes such as fossil fuel burning, municipal waste incineration, and water chlorination, although it is also intentionally employed as a pesticide, herbicide, fungicide, wood preservative, and reagent in organic synthesis.[4] The release of TCP into the environment has raised serious concerns for both ecological and human health. Its longevity is primarily due to the strong carbon–chlorine bonds, which are highly resistant to natural degradation processes.[5] As a result, TCP can persist for decades in water, soil, and sediments. Moreover, its ability to penetrate biological membranes and accumulate in tissues, even at trace levels, further amplifies its toxicological risk. TCP exposure is linked to serious health risks,[6,7] including carcinogenicity,[8] mutagenicity[9] and endocrine disruption.[10] In humans, it has been linked to respiratory and neurological disorders, including chronic bronchitis, cognitive impairment, and inhibition of acetylcholinesterase activity, an enzyme critical to the nervous system.[11]

The bioaccumulative nature of TCP enhances its environmental impact, accumulating at peak predators and endangering biodiversity.[12] Aquatic ecosystems are especially vulnerable, as TCP interferes with the metabolism and reproductive systems of aquatic organisms.[13] Owing to its toxicological properties and long-term persistence, TCP has been designed as a priority pollutant by the US Environmental Protection Agency (EPA) and the European Union. These classifications underscore the need for effective monitoring, regulation, and remediation strategies to mitigate its environmental and public health impacts.[14]

To address TCP pollution, various removal methods have been investigated. Among them, adsorption has gained

[a]*Chemistry Department, College of Science, University of Bahrain, Sakhir 32038, Kingdom of Bahrain. E-mail: ahmohamed@uob.edu.bh*

[b]*Inorganic Chemistry and Environment laboratory, University of Tlemcen, P. O. Box 119, 13000 Tlemcen, Algeria*

[c]*Department of Chemistry, Faculty of Science, Ain Shams University, Cairo 11566, Egypt. E-mail: ahkamel76@sci.asu.edu.eg*

prominence due to its efficacy, low energy demands, and cost-effectiveness.[15] Unlike other treatment options such as chemical oxidation or membrane filtration, which may produce harmful byproducts or involve high energy consumption, adsorption offers a simpler and environmentally safer alternative.[16] However, many traditional adsorbents are synthetic, expensive, and difficult to scale. In contrast, biosorption—which utilizes biological materials, particularly agricultural waste—offers a more sustainable and economical approach.[17] Among biosorbents, eggshells have emerged as promising candidates due to their high calcium carbonate ($CaCO_3$) content (~96%), which provides a favorable matrix for adsorbing organic pollutants like TCP.[18] Utilizing eggshells in water treatment simultaneously addresses two environmental challenges: food waste valorization and water pollution remediation.[19]

To enhance the adsorption performance of eggshells, chemical modification techniques such as acid activation can be employed. Acid-Activated Eggshell (AAES) is a modified material in which surface porosity and reactive sites are improved, thereby increasing its adsorption potential.[20] Furthermore, graphene oxide (GO) has demonstrated excellent adsorption characteristics due to its large surface area and abundant functional groups, which enable strong interactions with organic contaminants.[21] By integrating AAES with GO, a composite material (AAES/GO) can be fabricated that combines the advantageous properties of both components to achieve superior pollutant removal performance.

Our research focuses on the creation of an adsorbent composite consisting of chemically activated eggshells and graphene oxide (AAES/GO) for the removal of TCP. Our goal was to increase the adsorption capacity of the modified eggshells incorporated with GO by enhancing surface reactivity and porosity. The performance of the adsorbent in removing TCP was evaluated. The results of this study demonstrate not only the outstanding adsorption capacity of AAES/GO composite, but also its potential to be considered as an eco-friendly and efficient adsorbent for water contaminated by organic substances like TCP.

Materials and methodology

Apparatus

The structural, textural, and morphological properties of the AAES/GO composite were characterized using multiple advanced techniques. FTIR spectroscopy (SP3-300, Pye-Unicam, UK) was conducted in the 600–4000 cm^{-1} range using KBr pellets with a resolution of 4 cm^{-1} to identify functional groups and chemical bonding. X-ray diffraction (XRD) patterns were recorded using a Rigaku Ultima IV diffractometer equipped with Cu-Kα radiation ($\lambda = 1.5406$ Å), operated at 40 kV and 30 mA, over a 2θ range of 10–80° at a scan rate of 2° min^{-1}. Measurements were conducted at room temperature (~25 °C). Surface morphology was examined using a field emission scanning electron microscope (FE-SEM, JEOL JSM-7100F) at 15 kV. Samples were sputter-coated with a thin gold layer to enhance conductivity prior to imaging.

Chemicals and reagents

All chemicals used were of analytical grade and used without further purification. Graphene oxide powder (15–20 sheets, 4–10% edge-oxidized, avg. no. of layers, 15–20), sodium hydroxide (NaOH), hydrochloric acid (HCl), and phosphoric acid (H_3PO_4, 98%) were obtained from Sigma-Aldrich (Saint Lois, USA). 2,4,6-Trichlorophenol ($C_6H_3Cl_3O$, 97%) was obtained from Fluka Chemika. Ultrapure water was utilized for the preparation of all solutions.

Synthesis of AAES/GO composite

Eggshells were thoroughly washed, dried at 60 °C for 24 hours, ground, and sieved into a fine powder. The powder was soaked in 1 M H_3PO_4 for chemical activation to increase porosity and surface reactivity, then calcined at 500 °C for 2 hours. Simultaneously, graphene oxide was dispersed in ultrapure water *via* ultrasonic treatment (40 kHz, 30 min). The activated eggshell powder was then mixed with the GO dispersion under magnetic stirring for 1 hour. The AAES/GO ratio of 1 : 1 was selected because it yielded the best results in terms of adsorption efficiency during preliminary tests. Further studies are needed to optimize other ratios. The mixture was filtered, dried at 100 °C to remove residual moisture, and stored for further use.

Point of zero charge (PZC)

The PZC of the AAES/GO composite was determined using the salt addition method. A series of 50 ml 0.01 M NaCl solutions were adjusted to initial pH values ranging from 2 to 11 using 0.1 M HCl or NaOH. Then, 0.1 g of the AAES/GO composite was added to each solution and stirred for 24 hours at room temperature. The final pH values were recorded, and PZC was determined as the point where the difference between initial and final pH was zero.

Adsorption studies

Adsorption experiments were conducted step by step to explore the adsorption of 2,4,6-trichlorophenol (TCP) by AAES/GO composite as an adsorbent. Different amounts of AAES/GO composite (ranged from 5 to 60 mg) were dispersed in 25 ml of different 2,4,6-TCP concentrations (1 to 10 μg ml^{-1}) at pH 6.5. The mixtures were left under shaking using a mechanical shaker for a period starting from 1 min to 60 min at ambient temperature (~25 °C). After the isolation of the adsorbent, the concentration of the remaining 2,4,6-TCP in the resulting filtrate was detected using UV-vis spectrophotometer (Genesys 10S, USA) at $\lambda_{max} = 312$ nm.

Upon achieving equilibrium, eqn (1) and (2) were used to calculate the adsorption capacity (mg g^{-1}) and removal efficiency (%) of the prepared adsorbent.

$$Q_e = (C_o - C_e) \times V/M \quad (1)$$

$$\text{Removal efficiency (\%)} = (C_o - C_e)/C_o \times 100 \quad (2)$$

where C_o represents the initial concentration of 2,4,6-TCP (μg ml^{-1}), C_e is the concentration of 2,4,6-TCP at equilibrium (μg

ml^{-1}), V is the test solution volume of 2,4,6-TCP, and M is the mass of the adsorbent (g).

The effect of the test solution pH on the efficiency of the adsorption process was examined by mixing a 40 mg portion of the composite with 25 ml of the 2,4,6-TCP (10 μg ml^{-1}). The pH was adjusted at 2 to 10 using diluted HCl and/or NaOH. The removal efficiency of 2,4,6-TCP at each pH was calculated using eqn (2).

Adsorption kinetics

The adsorption kinetics of 2,4,6-TCP using AAES/GO composite was investigated by mixing 40 mg portion of the composite with a 25 ml aliquot of 2,4,6-TCP (10 μg ml^{-1}) at pH 6.5. The mixture was stirred for 1 to 60 min. The adsorption rate was determined through fitting the experimental data with pseudo-first-order and pseudo-second-order models, using eqn (3) and (4), respectively.[22]

$$\log(Q_e - Q_t) = \log Q_e - \frac{K_1}{2.303} t \quad (3)$$

$$\frac{t}{Q_t} = \frac{1}{K_2 Q_e} + \frac{t}{Q_e} \quad (4)$$

where Q_t (mg g^{-1}) is the amount of 2,4,6-TCP adsorbed at time t (min), and Q_e (mg g^{-1}) is the adsorption capacity at equilibrium. k_1 (min^{-1}) and k_2 (g mg^{-1}. min^{-1}) are the adsorption rate constants associated with the pseudo-first-order and pseudo-second-order models, respectively.

Adsorption isotherms

The adsorption isotherms were investigated by mixing 40 mg of AAES/GO composite with 25.0 ml portions of aqueous 2,4,6-TCP solution having different concentrations (1 to 10 μg ml^{-1}) at pH 6.5. After a 10-min stirring period, the AAES/GO composite was filtered and the remaining 2,4,6-TCP concentration was determined by spectrophotometric absorption technique at λ_{max} = 312 nm. The data obtained were then fitted and compared with Langmuir, Freundlich, and Temkin,[23] expressed by eqn (5), (6), and (7), respectively.

$$(C_e/Q_e) = (1/a_L\ Q_{max}) + (C_e/Q_{max}) \quad (5)$$

$$\log Q_e = \log k_F + (1/n) \log C_e \quad (6)$$

$$Q_e = RT/B_T \ln C_e + RT/B_T \ln K_T \quad (7)$$

where C_e (μg ml^{-1}) is the equilibrium concentration of 2,4,6-TCP, Q_e (mg g^{-1}) is the adsorption capacity at equilibrium, and Q_{max} (mg g^{-1}) is the maximum adsorption capacity of the adsorbent. The Langmuir constant is represented by a_L, the Freundlich constant by k_F, and $(1/n)$ is the heterogeneity factor. T is the absolute temperature, R is the gas constant, B_T is Temkin constant), K_T is the Temkin isotherm constant.

Results and discussions

Characterization of the synthesized AAES/GO composite

FTIR spectroscopy. The FTIR spectra of AAES, GO, and the AAES/GO composite are presented in Fig. 1. Characteristic

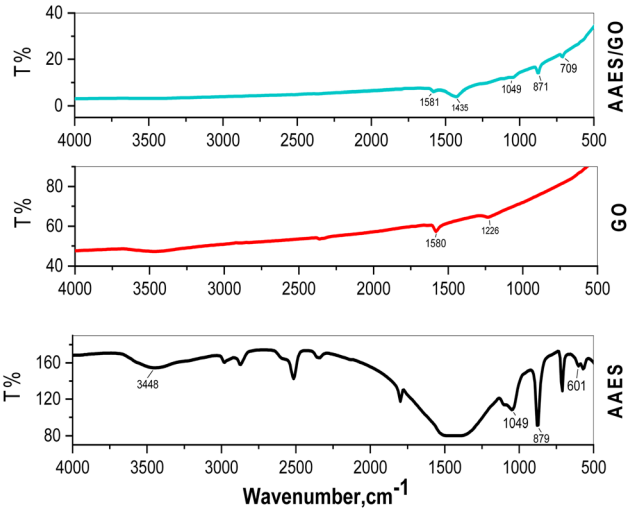

Fig. 1 FTIR spectra of AAES, GO and AAES/GO composite.

absorption bands confirm the functional groups present in the individual components and the composite. For AAES, absorption bands were observed at ν_{max} cm^{-1} 875 and 1420, which are attributed to the out-of-plane bending and asymmetric stretching vibrations of carbonate groups (CO_3^{2-}), confirming the presence of calcium carbonate, the primary constituent of eggshells. Additionally, a broad band at ν_{max} cm^{-1} 3400 is assigned to O–H stretching, formed during acid activation with H_3PO_4, which introduces phosphate groups that interact with water during washing to produce surface hydroxyl groups, and a peak at 1650 corresponds to C=O stretching, likely due to acid activation. For graphene oxide (GO), a broad absorption band appeared at ν_{max} cm^{-1} 3460–3200, assigned to O–H stretching vibrations. The band at ν_{max} cm^{-1} 1720 is attributed to C=O stretching of carboxylic groups, while bands at 1220 and 1050 are assigned to C–O stretching vibrations of epoxy and alkoxy groups, respectively. In the AAES/GO composite, the spectrum displays a superposition of characteristic bands from both AAES and GO, with slight shifts in peak positions and intensity variations, indicating interactions such as hydrogen bonding between the –OH groups in AAES and the oxygen-containing functional groups of GO. These spectral modifications confirm the successful integration and interaction between the two components in the composite structure.

Morphological structure using SEM analysis. As shown in Fig. 2, there is a significant morphological difference between AAES and the AAES/GO composite. In the SEM image of AAES (Fig. 2a), the particles exhibit an irregular shape with diameters ranging from 1.287 to 1.827 μm. Their rough surface is indicative of the porous structure formed after acid activation. In contrast, the AAES/GO composite presents a more compact and agglomerated structure, with an increased particle size of approximately 2.590 μm (Fig. 2b). The presence of graphene oxide (GO) seems to promote the clumping of AAES particles, leading to a denser and more stable composite material. This structural transformation suggests that GO not only modifies the morphology of AAES but may also enhance its adsorption capacity or other functional properties.

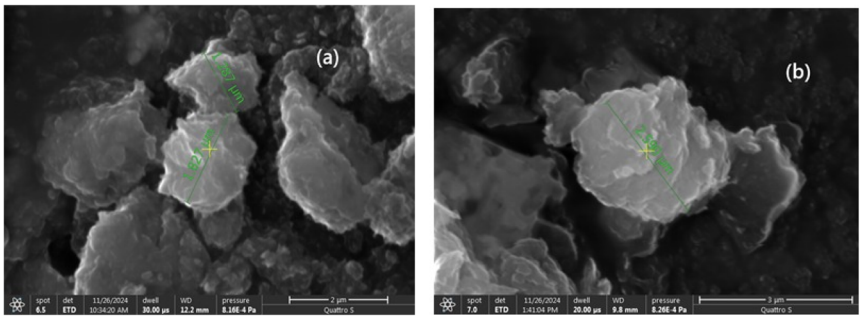

Fig. 2 SEM images of AAES (a) and AAES/GO composite (b) (X50000).

Structural composition. The crystallinity and structural features of the synthesized AAES/GO composite were investigated by X-ray diffraction (XRD) and energy-dispersive X-ray spectroscopy (EDX). The XRD patterns of GO, AAES, and the AAES/GO composite are shown in Fig. 3. For graphene oxide (GO), a broad diffraction peak was observed at $2\theta \approx 10.8°$, which corresponds to the (001) reflection, indicative of the interlayer spacing due to oxygen-containing functional groups and the disordered arrangement of GO sheets, consistent with the literature [JCPDS No. 40-0019]. In the case of acid-activated eggshell (AAES), the diffraction pattern exhibited sharp reflections primarily assigned to hexagonal calcite $CaCO_3$. The prominent peak at $2\theta \approx 29.5°$, indexed to the (104) plane, corresponds to calcite structure of $CaCO_3$ (JCPDS No. 47-1743). The increased intensity of this peak in the AAES/GO composite suggests recrystallization and improved phase alignment due to acid activation followed by thermal treatment, as well as potential orientation effects upon composite formation. The XRD pattern of the AAES/GO composite revealed characteristic diffraction peaks at $2\theta = 25.0°$ (012), 29.5° (104), 35.9° (110), 39.4° (113), 43.1° (202), 48.5° (116), 56.6° (211), 57.4° (122), and 63.1° (125), confirming the retention of the calcite phase in the composite structure. These peaks match well with the standard reference data for hexagonal $CaCO_3$ (JCPDS No. 47-1743), verifying the structural integrity of the eggshell-derived component. Furthermore, the overlay of AAES and GO diffraction features, along with slight shifts and changes in intensity, points to structural interactions between the $CaCO_3$ matrix and the GO sheets. These may include hydrogen bonding, electrostatic interactions, or partial chemical incorporation of GO within the porous AAES framework, contributing to slight lattice distortions and peak broadening. Together, the XRD findings confirm the successful integration of GO into the AAES matrix while retaining the crystallographic identity of the $CaCO_3$ phase, supporting the formation of a structurally stable and functional composite adsorbent.

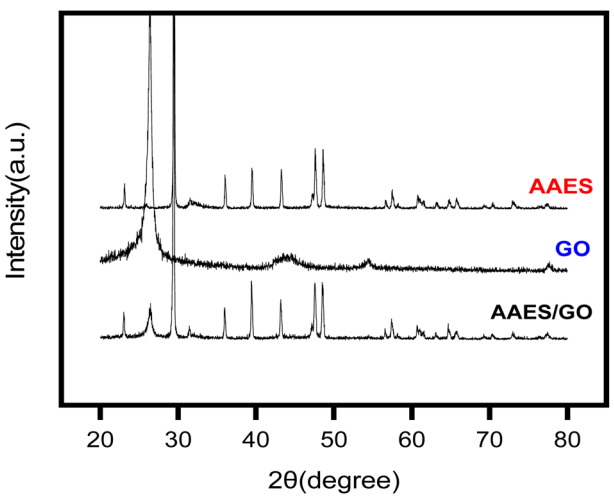

Fig. 3 XRD patterns of GO, AAES and AAES/GO.

As shown in Table 1, the Energy Dispersive X-ray (EDX) analysis confirms the successful incorporation of graphene oxide (GO) into the AAES/GO composite by revealing distinct changes in the elemental composition. The primary elements in AAES include calcium (Ca), oxygen (O), carbon (C), and phosphorus (P). The presence of phosphorus is attributed to the activation process with phosphoric acid (H_3PO_4), where phosphate groups are incorporated into the material structure (Fig. 4b). A notable increase in carbon content, from 34.8% in AAES to 52.0% in AAES/GO, is observed (Fig. 4b). This directly correlates with the contribution of carbon from GO. Simultaneously, oxygen content decreases from 43.0% to 32.4%, which may be due to the dilution of oxygen-containing functional groups in AAES following GO addition or partial reduction of GO during composite synthesis. Additionally, the calcium content exhibits a slight decrease, from 18.7% to 15.6%, reflecting a dilution effect in the composite matrix. The disappearance of phosphorus in the AAES/GO composite suggests either an even distribution of phosphate groups, making them less detectable, or that GO dominates the analyzed sample composition. These findings confirm that GO integration alters the elemental composition of AAES while maintaining its structural integrity, ensuring the preservation of H_3PO_4-induced activation characteristics.

Adsorption–desorption isotherm and pore structure. The surface characteristics of the Acid-Activated Eggshell (AAE) and AAE/Graphene Oxide (GO) composite were analyzed by nitrogen adsorption–desorption isotherms at 77.4 K using the BET method. Prior to analysis, all samples were degassed at 200 °C for 2 hours to remove residual moisture and gases. Fig. 5 presents the N_2 adsorption–desorption isotherms. Both

Table 1 Elemental composition of pure AAES and AAES/GO composite with observed changes

Element	Pure AAES (% by weight)	AAES/GO (% by weight)	Change
C (carbon)	34.8%	52.0%	Increase (+17.2%)
O (oxygen)	43.0%	32.4%	Decrease (−10.6%)
Ca (calcium)	18.7%	15.6%	Slight decrease (−3.1%)
P (phosphorus)	3.2%	Not detected	Disappearance

Table 2 Surface parameters of the synthesized AAE (Acid-Activated Eggshell) and AAE/GO composite obtained by BET method

Property	AAE (Acid-Activated Eggshell)	AAE/GO composite
Surface area ($m^2\ g^{-1}$)	118	224
Pore volume ($cm^3\ g^{-1}$)	0.21	0.19
Pore diameter (nm)	7.1	6.2
Dominant pore type	Mesoporous (BJH: 4–20 nm)	Mesoporous (BJH: 3–15 nm)

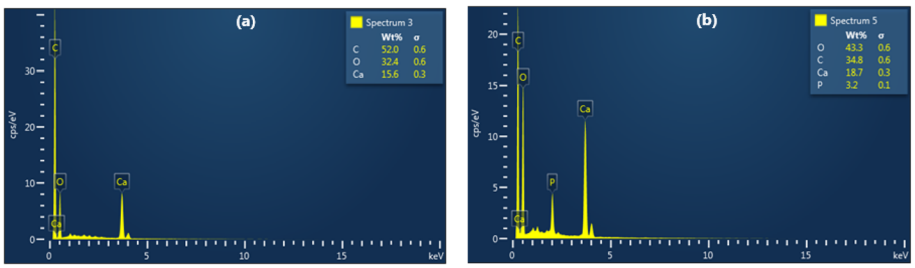

Fig. 4 EDX spectra of: (a) AAES/GO composite; and AAES.

materials display isotherms with a steep increase in volume adsorbed at high relative pressure ($p/p_0 \approx 0.9$–1.0), which may suggest the presence of large mesopores or macroporous voids. A clearly defined hysteresis loop—typical of classical Type IV isotherms—is not prominent. Thus, the materials exhibit mixed porosity characteristics, likely with dominant mesopores and some contribution from interparticle macroporosity. Based on BET analysis, the surface area of AAE was determined to be 118 $m^2\ g^{-1}$, which increased to 224 $m^2\ g^{-1}$ after incorporation of

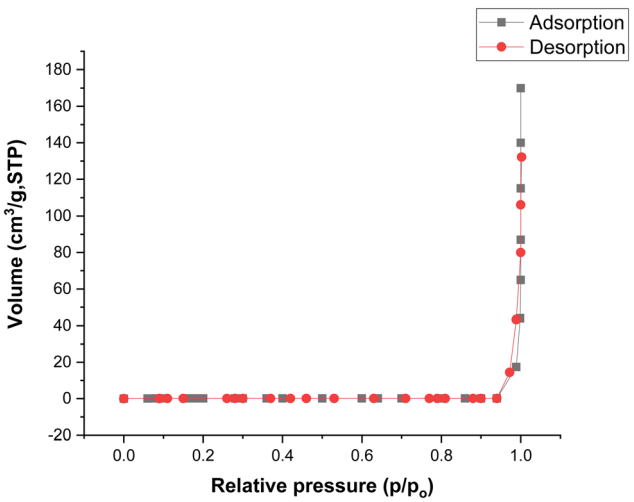

Fig. 5 Nitrogen adsorption–desorption isotherm of AAE/GO composite.

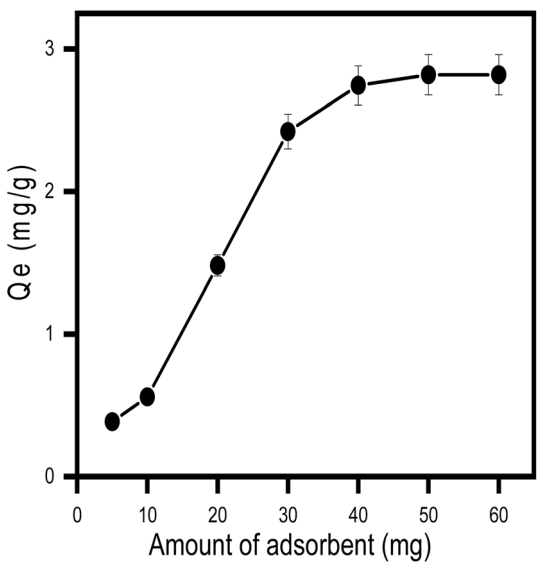

Fig. 6 Adsorption of 2,4,6-TCP on the AAES/GO composite as a function of amount [experimental conditions: the concentration of 2,4,6-TCP = 10 μg ml^{-1}, contact time = 10 min, volume of test solution = 25 ml at pH = 6.5] Effect of initial concentration of 2,4,6-TCP.

GO. This enhancement is attributed to the high specific surface area and exfoliated structure of GO, which provides additional adsorption sites. The average pore diameters calculated by BJH method were 7.1 nm for AAE and 6.2 nm for AAE/GO, confirming the presence of mesopores. Pore volume also showed slight variations (AAE: 0.21 cm^3 g; AAE/GO: 0.19 cm^3 g^{-1}), potentially due to partial pore blockage by GO sheets. These results suggest that the improved surface area and preserved mesoporosity in the composite contribute to its enhanced adsorption capacity for organic pollutants such as 2,4,6-trichlorophenol.

Adsorption studies

Effect of adsorbent dose. Different quantities of the synthesized AAES/GO composite adsorbent (5–60 mg) were mixed with 25 ml aliquots of 2,4,6-TCP test solution (10 μg ml^{-1}) at pH 6.5 and shaken for 10 min. The optimum quantities of the adsorbent for achieving maximum efficiency of the removal of 2,4,6-TCP are presented in Fig. 6. The results obtained clearly demonstrate that as the proposed synthesized AAES/GO composite adsorbent dosage increased, the equilibrium adsorption capacity (Q_e) improved until reaching a maximum of 2.5 mg g^{-1} with a dose of 40 mg. Beyond this point, Q_e plateaus due to the limited availability of 2,4,6-TCP molecules in the solution, as the fixed pollutant concentration (10 μg ml^{-1}) is fully utilized by the available active sites. These results indicated that AAES/GO composite exhibited a synergistic effect, resulting in enhanced adsorption of 2,4,6-TCP.

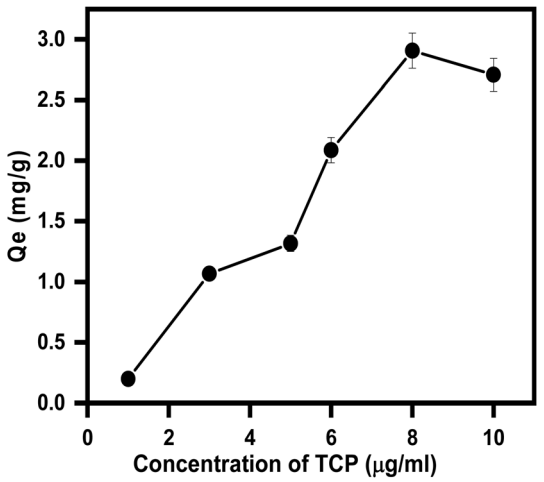

Fig. 7 Adsorption of 2,4,6-TCP on the AAES/GO composite as a function of concentration [experimental conditions: adsorbent dose = 40 mg, contact time = 10 min, volume of test solution = 25 ml at pH = 6.5].

Under the optimized adsorption conditions, the effect of the initial 2,4,6-TCP concentration (ranging from 1.0 to 10.0 μg ml^{-1}) on the equilibrium adsorption capacity (Q_e) was examined. As shown in Fig. 7, the results revealed a continuous increase in the equilibrium adsorption capacity (Q_e) of the adsorbent as the initial 2,4,6-TCP concentration increases due to the enhancement of the availability of molecules to interact with the adsorbent. By raising the concentration, the driving force for mass transfer (concentration gradient) will be greater, which facilitates the movement of the TCP molecules to the active sites on the composite. Once the concentration reaches a certain level (around 8 μg ml^{-1}), a plateau is achieved when all active binding adsorption sites on the AAES/GO composite were saturated with 2,4,6-TCP. At 10.0 μg ml^{-1}, a slight decrease in Q_e was observed, likely due to the limited density of accessible adsorption sites on the composite's mesoporous structure, which restricts further uptake of TCP molecules despite the increased concentration. It was noticed that the equilibrium adsorption capacity (Q_e) of the proposed AAES/GO composite sorbent was 2.55 ± 0.6 mg g^{-1}. This value indicated a good efficiency of the proposed composite in removing 2,4,6-TCP from industrial wastewater samples.

Effect of pH. The effect of pH on the adsorption efficiency of AAES/GO composite for the removal 2,4,6-TCP was tested over the pH range of 2 to 10. As shown in Fig. 8a, the results revealed that, at pH < 4, the equilibrium adsorption capacity (Q_e) was low (1.0 mg g^{-1}). At pH > 5, the adsorption capacity, reaching a maximum of 2.65 mg g^{-1} at pH 6.5. There was a notable

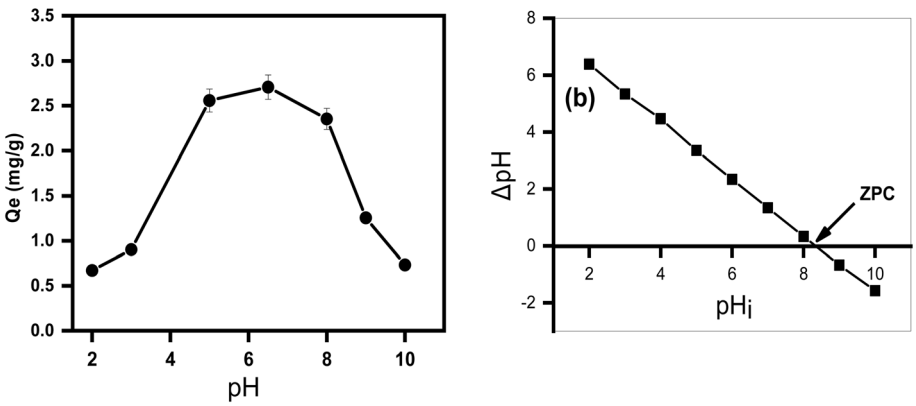

Fig. 8 (a) Influence of pH on the adsorption efficiency of 2,4,6-TCP from aqueous solutions using AAES/GO composite [experimental conditions: initial 2,4,6-TCP concentration = 10 μg ml^{-1}, volume of test solution = 25 ml, contact time = 10 min, and adsorbent dose = 40 mg]. (b) Point of zero charge (PZC) plot of AAES/GO composite.

decrease in removal efficiency above pH 7, probably due to the formation of 2,4,6-trichlorophenolate ion. The point of zero charge (PZC) of the AAES/GO composite measurement was determined and found to be at pH = 8.0 (Fig. 8b). This indicated that the adsorbent surface became positively charged at pH < 8.0 probably due to H^+ adsorption over the adsorbate surface. At pH > 8, the surface charge develops negative character which will decrease the adsorption efficiency due to the possible repulsion between this negatively charged surface and 2,4,6-trichlorophenolate ion formed (pK_a of 2,4,6-TCP is 6.23). In conclusion, the observed pH-dependent adsorption behavior of the AAES/GO composite for 2,4,6-TCP can be explained by electrostatic interactions and ionization effects. At low pH (<4), the low equilibrium adsorption capacity (Q_e = 1.0 mg g^{-1}) is likely due to protonation of functional groups on the adsorbent surface, which reduces available active sites for 2,4,6-TCP interaction. The increase in adsorption at pH 5–6.5 (maximum Q_e = 2.65 mg g^{-1} at pH 6.5) corresponds to a favorable charge interaction between the partially ionized 2,4,6-TCP molecules and the positively charged adsorbent surface. However, at pH > 7, the adsorption efficiency declines due to the formation of 2,4,6-trichlorophenolate ions, which experience electrostatic repulsion from the negatively charged surface of the adsorbent (above its point of zero charge, pH 8.0). These results indicate that electrostatic attraction is the dominant adsorption mechanism at acidic to near–neutral pH, while charge repulsion limits adsorption at higher pH levels.

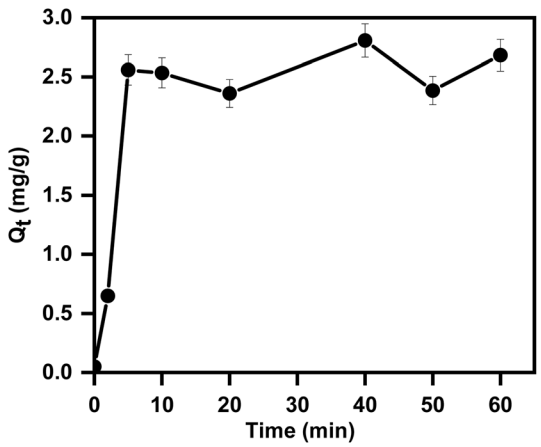

Fig. 9 Adsorption of 2,4,6-TCP on the AAES/GO composite as a function of time [experimental conditions: adsorbent dose = 40 mg, initial concentration = 10 μg ml^{-1}, volume of test solution = 25 ml at pH = 6.5].

Kinetic study on the adsorption process. A correlation was made between the adsorption efficiency of 2,4,6-TCP using the synthesized AAES/GO composite and the contact time. As shown in Fig. 9, the adsorption of 2,4,6-TCP revealed an increase over time reaching an equilibrium at nearly 10 min with a maximum adsorption capacity Q_{max} = 2.65 mg g^{-1}. This may be due to the high availability of the active sites on the composite surface. These sites, located on the surface and easily accessible pores, allow quick interaction with TCP molecules in the solution. After 10 min, adsorption reaches a plateau at a maximum adsorption capacity Q_{max} = 2.9 mg g^{-1}. This slowing down is due to the progressive saturation of active sites. At this stage, only TCP molecules capable of penetrating deeper into the porous structure or finding remaining internal sites can be adsorbed, which is a slower process.

Pseudo-first order and pseudo-second-order models were used to investigate the kinetics of the adsorption of 2,4,6-TCP by the synthesized AAES/GO composite. Fig. 10a and b illustrate the fitting of the experimental kinetic data for Pseudo-first order

Table 3 The kinetic parameters calculated using the pseudo-first-order and pseudo-second-order models in the linear forms

Adsorption kinetic model	Parameters	Value
Pseudo-first-order	k_1, min^{-1}	0.24
	Q_{e1}, mg g^{-1}	2.5
	R^2	0.97
Pseudo-first-order	k_2, g mg^{-1} min	0.74
	Q_{e2}, mg g^{-1}	2.67
	Qeexp, mg g^{-1}	2.81
	R^2	0.99

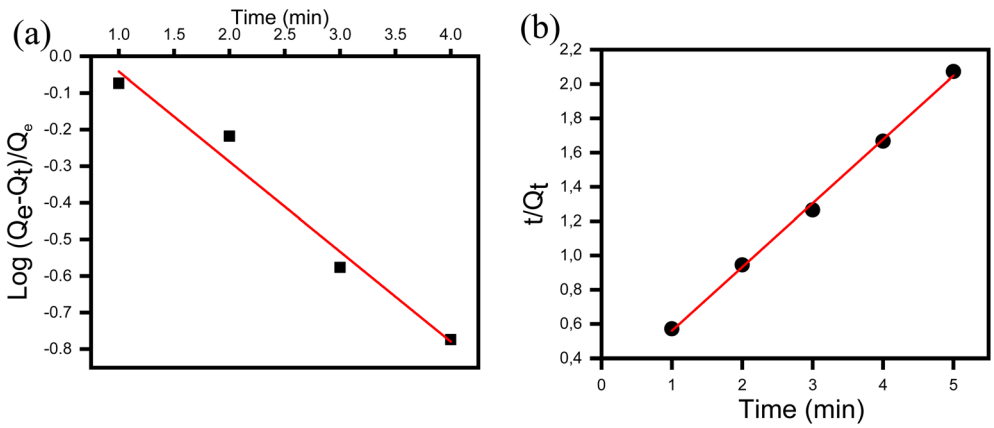

Fig. 10 Fitting plots of adsorption kinetics using pseudo-first-order (a) and pseudo-second-order (b) models for 2,4,6-TCP adsorption on AAES/GO composite.

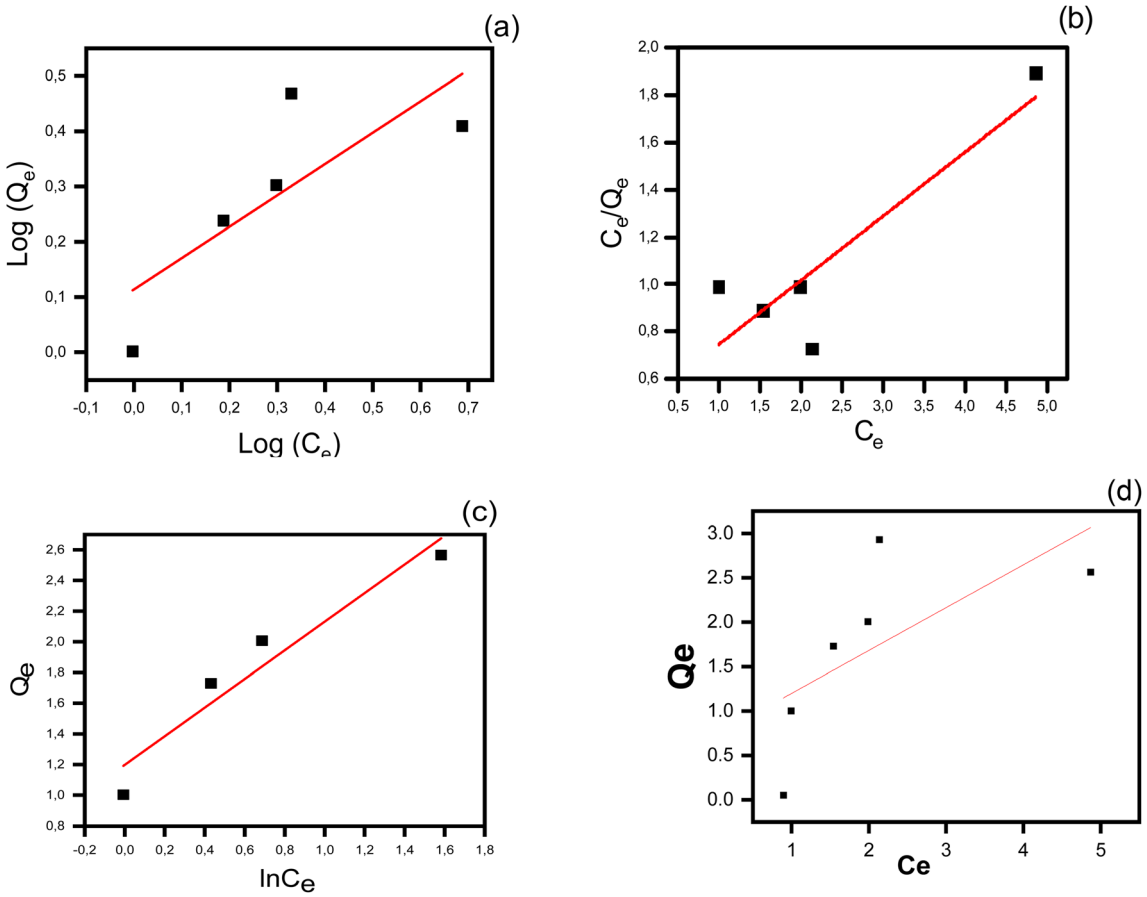

Fig. 11 Freundlich (a), Langmuir (b), and Temkin (c), adsorption isotherm models for the removal of 2,4,6-TCP on the AAES/GO composite; (d) Q_e *vs.* C_e plot.

and pseudo-second-order models, respectively. The results presented in Table 3 indicated a higher correlation coefficient (R^2) for the pseudo-second-order model when compared with the pseudo-first-order model. A further confirmation was obtained by calculation of the adsorption capacities ($Q_e{}^2$ and Qeexp), where a close match with pseudo-second-order model values were obtained.

The pseudo-second-order model that is based on specific chemical interaction between 2,4,6-TCP and the composite suits the process more ($R^2 = 0.99$). It indicates that the adsorption mechanism is dominated by chemisorption, in which electron transfer or specific chemical bonding occurs. The good fit to the pseudo-second-order model further supports that chemical interaction plays a significant role in the adsorption of TCP on the AAES/GO composite. The likely mechanisms involve specific chemical bonds, in which functional groups in 2,4,6-TCP (such as hydroxyl and aromatic groups) may strongly interact with AAES active sites (phosphate groups) or GO active sites (carboxyl and hydroxyl groups). The bonds are complemented by the nature of GO, which increases the active site density on the composite. Also playing a part are π–π interactions as the aromatic ring of TCP can interact *via* π–π stacking with the sp^2 areas of GO, an effective way of adsorbing aromatic organic compounds such as TCP.

Adsorption isotherms. Several adsorption isotherm models, including Langmuir, Freundlich, and Temkin, were assessed and fitted to the obtained data, as shown in Fig. 11. The results in Table 4 revealed that the Freundlich model with a correlation coefficient of ($R^2 = 0.62$), signifies an approximately favorable adsorption ($K_F = 1.29$), ($1/n = 0.56$) on a heterogenous surface despite being the worst fit of these models. The contrast, however, is the Langmuir isotherm that better explains ($R^2 =$

Table 4 Adsorption isotherm parameters obtained using Langmuir, Freundlich, and Temkin, and for the adsorption of 2,4,6-TCP onto the AAES/GO composite

Freundlich isotherm			Langmuir isotherm			Temkin isotherm		
R^2	K_F	$1/n$	R^2	Q_{max} (mg g^{-1})	K_L (L mg^{-1})	R^2	K_t (L mg^{-1})	B (L g^{-1})
0.62	1.29	0.56	0.78	3.69	2.11	0.92	3.61	0.93

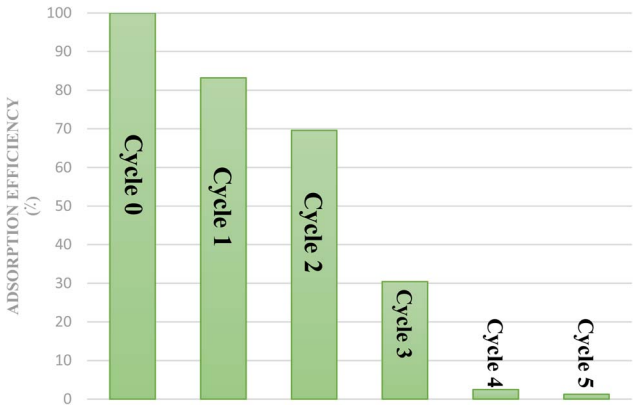

Fig. 12 Regeneration studies of AAES/GO composite.

0.78), the adsorption as homogeneous with a maximum capacity of 3.69 mg g^{-1} and affinity parameter of (K_L = 2.11 L mg^{-1}). Finally yet importantly, the Temkin isotherm that best explains (R^2 = 0.92), the adsorption as adsorbate–adsorbent interaction-influenced and parameterized by (K_T = 3.61 L mg^{-1}) and (B = 0.93 L g^{-1}), denotes moderately favorable and energetically efficient adsorption. Consequently, the Temkin model is the most common, and it focuses on the significance of molecular interactions during adsorption.

Adsorbent regeneration. Regeneration of the AAES/GO composite was performed under the best conditions, confirming its regeneration ability. The composite was harvested after each adsorption cycle, washed with distilled water to remove any remaining pollutants, and dried before reuse, showing reproducible performance in repeated cycles. Nevertheless, as shown in Fig. 12, the adsorption efficiency gradually reduced with each subsequent cycle. At Cycle 0 (the first adsorption cycle), in an ideal scenario, the composite had reached 99.8% efficiency after 10 minutes and was a control to be used for comparison purposes. The efficiency declined to 83% in Cycle 1 (first regeneration cycle), demonstrating successful regeneration. During the second cycle, efficiency fell a bit to 70%, demonstrating some decline in performance but active. A steep fall was observed in the third cycle, where the efficiency fell to 31%, which may be due to active site degradation. In the fourth and fifth cycles, adsorption efficiency fell below 5%, rendering the composite useless. Despite this decline, the results show that the AAES/GO composite remains a promising candidate for adsorption applications since it can be reused efficiently at least two to three times with comparatively high efficiency. Its reusability suggests its potential as a cost-effective and environmentally friendly method for the removal of pollutants, although material degradation with time cannot be prevented.

Mechanism of adsorption. The adsorption of 2,4,6-trichlorophenol (2,4,6-TCP) onto the AAES/GO composite is proposed to occur *via* multiple synergistic interactions, as illustrated in Fig. 13. At pH < 6.5, 2,4,6-TCP exists in both neutral (TCP) and ionized (TCP^-) forms due to its pK_a (~6.23), and the removal process is governed by a combination of mechanisms. First, π–π stacking interactions occur between the aromatic ring of TCP and the sp^2-hybridized carbon domains of graphene oxide (GO), as commonly reported for carbon-based adsorbents used to capture chlorinated organics.[21] Second, hydrogen bonding arises between the hydroxyl group of TCP and the oxygen-containing functional groups (–COOH, –OH, –C=O) on GO, supported by FTIR spectral shifts observed in the composite and similar to those reported in GO-based sorbents.[22] Third, the negatively charged TCP^- species interact electrostatically with Ca^{2+} ions present on the AAES surface, where calcium acts as a Lewis acid capable of binding anionic species.[24] Additionally, surface complexation may occur between GO's carboxyl groups and AAES-derived Ca^{2+} ions, further stabilizing the composite and promoting organized binding sites.[26] These interactions act cooperatively, resulting in enhanced removal efficiency through increased surface reactivity and multi-site binding. This mechanism explains both the high uptake capacity and the observed pH dependence of the composite during TCP adsorption.

Comparison with different adsorbents for 2,4,6-trichlorophenol removal. Table 5 illustrates the adsorption

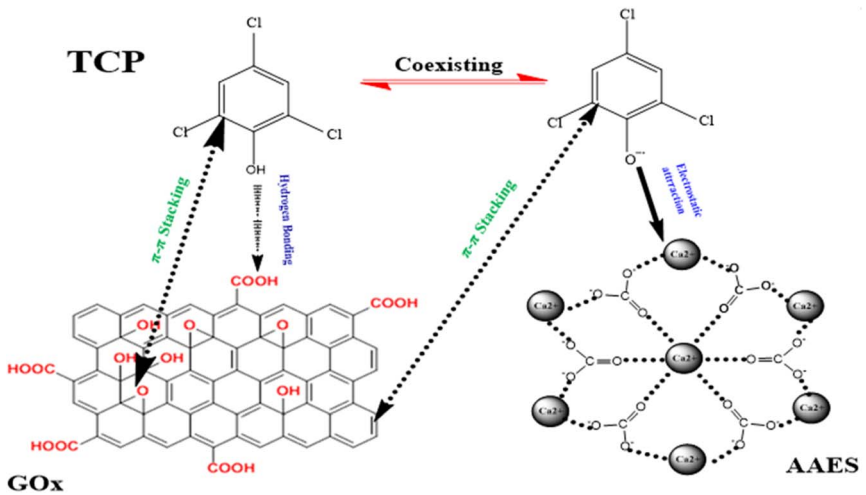

Fig. 13 Proposed adsorption mechanism of 2,4,6-TCP on AAES/GO composite.

Table 5 Comparison of maximum adsorption capacity of 2,4,6-trichlorophenol on various adsorbents

Adsorbents	Removal percentage (%)	Initial concentration, mg L^{-1}	Adsorption isotherm	Optimum pH	Adsorbent dosage, mg mL^{-1}	Agitation time, min	Ref.
Activated carbon from coconut shell	99.8	50	Freundlich	2	500 mg/100 ml	210	25
Activated carbon prepared from oil palm empty fruit bunch	—	250	Freundlich and Redlich–Peterson	2	100/100 ml	300–360	27
Bentonite modified	99.5	50	Langmuir and Freundlich	4	70 mg/50 ml	60	28
AAES/GO	99.7	10	Temkin	6.5	40 mg/25 ml	10	This work

efficiency (R%) of various adsorbents for pollutant removal, as documented in the literature. The findings reveal that the AAES/GO material developed in this study achieved a maximum adsorption yield of 100% under optimized conditions, which included a neutral pH, an adsorbent weight of 50 mg, and an exceptionally brief adsorption duration of only 10 minutes. In contrast, other adsorbents, while highly effective (with R% values ranging from 95.5% to 99.8%), did not reach this level of efficiency. These results affirm the superiority of AAES/GO, emphasizing its potential as a highly effective adsorbent for rapid and cost-effective environmental applications.

Conclusion

The innovative AAES/GO composite synthesized from eggshells and graphene oxide demonstrates a promising approach for addressing TCP contamination in aquatic systems. Characterization studies confirmed the successful structural integration of GO into the AAES matrix, resulting in a composite with a high surface area (224 m^2 g^{-1}, Table 2). While individual adsorption data for GO and AAES were not provided in this study, the AAES/GO composite exhibited high adsorption efficiency (Q_e = 2.65 mg g^{-1}, 99.8% removal), suggesting that the combination of GO's surface area and AAES's porous structure may contribute to its performance, pending further comparative studies. Adsorption experiments revealed efficient TCP removal, governed primarily by chemisorption and π–π interactions, with optimal performance observed at neutral to alkaline pH levels. The adsorption process adhered to the pseudo-second-order kinetic model and Temkin isotherm, reflecting strong but reversible chemical interactions between TCP and the composite. However, adsorption capacity plateaued with increasing pollutant concentration, indicating saturation of active sites. Regeneration studies showed a gradual decline in efficiency after multiple cycles, suggesting the need for material optimization for long-term reuse. This work not only provides a sustainable solution for TCP removal but also valorizes eggshell waste, addressing dual environmental challenges.

Ethical statement

This article does not contain any studies with human participants or animals performed by any of the authors.

Data availability

Data will be made available on request.

Author contributions

Ayman H. Kamel: conceptualization, formal analysis, investigation, methodology, supervision, visualization, writing – original draft, writing – review & editing. Lina Adeida: formal analysis, investigation, methodology, writing – original draft. Belkacem Benguella and Makhoukhi Benamar: data curation, conceptualization, supervision, visualization, writing – original draft.

Conflicts of interest

The authors declare that the research was conducted in the absence of any commercial or financial relationships that could be construed as a potential conflict of interest.

Acknowledgements

The authors gratefully acknowledge the University of Bahrain, College of Science, Chemistry Department, for providing the laboratory facilities and support essential to the completion of this work.

References

1 Z. N. Garba, W. Zhou, I. Lawan, W. Xiao, M. Zhang, L. Wang, L. Chen and Z. Yuan, *J. Environ. Manage.*, 2019, **241**, 59.
2 Y. Peng, J. Chen, S. Lu, J. Huang, M. Zhang, A. Buekens, X. Li and J. Yan, *Chem. Eng. J.*, 2016, **292**, 398.
3 H. H. Shanaah, Z. Ameen, K. Jaafar, A. Hefnawy, H. S. M. Abd-Rabboh and A. H. Kamel, *ChemElectroChem*, 2023, **10**, e202300153.
4 B. Taqiyeddine, M. Ameri, N. Bouzouira, I. Ameri, L. F. Blaha, Y. Al-Douri, A. Bouhemadou, R. A. Al-Samarai and M. F. A. Alias, *Comput. Theor. Chem.*, 2024, **1239**, 114770.
5 J. Ou, R. Xian, J. Li, J. Zhao, K. Zhang, P. Mo, J. Fang, Y. Shen, X. Hu, S. Fang, W. Liu and H. Pan, *Ecotoxicol. Environ. Saf.*, 2024, **277**, 116345.

6 Y. Li, Y. Li, B. Jin, K. Zhang, L. Wang and J. Zhao, *Bioresour. Technol.*, 2021, **323**, 124627.
7 M. Wang, D. Ren, Z. Wang, Y. Li, S. Zhang, X. Gong and X. Zhang, *Catal. Commun.*, 2023, **184**, 106793.
8 M. R. Rooney, P. L. Lutsey, P. Bhatti and A. Prizment, *J. Occup. Environ. Med.*, 2019, **76**, 181.
9 A. M. Hammam, M. S. Zaki, R. A. Yousef and O. Fawzi, *Adv. Environ. Biol.*, 2015, **9**, 38+.
10 C. Yu, C. Wang, Z. Lu, C. Zhang, W. Dai, S. Yu, S. Lin and Q. Zhang, *Chemosphere*, 2019, **218**, 941.
11 E. O. Igbinosa, E. E. Odjadjare, V. N. Chigor, I. H. Igbinosa, A. O. Emoghene, F. O. Ekhaise, N. O. Igiehon and O. G. Idemudia, *Sci. World J.*, 2013, 2013.
12 C. A. M. van Gestel and W.-C. Ma, *Ecotoxicol. Environ. Saf.*, 1988, **15**, 289.
13 T. Ge, J. Han, Y. Qi, X. Gu, L. Ma, C. Zhang, S. Naeem and D. Huang, *Aquat. Toxicol.*, 2017, **184**, 78.
14 M. C. Díaz-Báez and J. D. Valderrama-Rincon, *J. Hazard. Mater.*, 2017, **324**, 599.
15 T. S. Hamidon and M. H. Hussin, *Int. J. Biol. Macromol.*, 2023, **233**, 123535.
16 R. Rashid, I. Shafiq, P. Akhter, M. J. Iqbal and M. Hussain, *Environ. Sci. Pollut. Res.*, 2021, **28**, 9050.
17 N. H. Solangi, J. Kumar, S. A. Mazari, S. Ahmed, N. Fatima and N. M. Mubarak, *J. Hazard. Mater.*, 2021, **416**, 125848.
18 V. K. Yadav, K. K. Yadav, M. M. S. Cabral-Pinto, N. Choudhary, G. Gnanamoorthy, V. Tirth, S. Prasad, A. H. Khan, S. Islam and N. A. Khan, *Appl. Sci.*, 2021, **11**, 4212.
19 J. Carvalho, J. Araujo and F. Castro, *Waste Biomass Valorization*, 2011, **2**, 157.
20 M. Ikram, A. U. Rehman, S. Ali, S. Ali, S. U. H. Bakhtiar, S. Alam and J. Biomed, *Eng. Inform.*, 2016, **2**, 118.
21 S. Verma and M. N. Nadagouda, *ACS Omega*, 2021, **6**, 4119–4125.
22 J. Wang and X. Guo, *J. Hazard. Mater.*, 2020, **390**, 122156.
23 M. Musah, Y. Azeh, J. Mathew, M. Umar, Z. Abdulhamid and A. Muhammad, *Caliphate J. Sci. Technol.*, 2022, **4**, 20.
24 M. Rani, U. Keshu and U. Shanker, *ChemistrySelect*, 2023, **8**, e202203540.
25 M. Radhika and K. Palanivelu, *J. Hazard. Mater.*, 2006, **138**, 116.
26 S. A. Hamza, S. Rasheed and A. Hussein, *J. Mech. Behav. Mater.*, 2022, **31**, 112.
27 I. A. W. Tan, A. L. Ahmad and B. H. Hameed, *J. Hazard. Mater.*, 2009, **164**, 473.
28 S. Ghezali, A. Mahdad-Benzerdjeb, M. Ameri and A. Z. Bouyakoub, *Chem. Int.*, 2018, **4**, 24.